



## Flow Field Study of Mixed Compression Supersonic Air Intake with Cowl Ventilation

N. K. Gahlot<sup>1,2</sup> and N. K Singh<sup>1†</sup>

<sup>1</sup>Department of Mechanical Engineering, National Institute of Technology, Kurukshetra, Haryana, 136119, India

<sup>2</sup>Department of Mechanical Engineering, SRM Institute of Science & Technology, Ghaziabad, Uttar Pradesh, 201204, India

†Corresponding Author Email:[nksinghfme@nitkkr.ac.in](mailto:nksinghfme@nitkkr.ac.in)

(Received February 1, 2020; accepted April 5, 2020)

### ABSTRACT

The present investigation is focused on the effect of cowl porosity on the performance of supersonic mixed compression air intake. Four different cases (namely 4.4 %, 5 %, 5.5 % and 7.2% of total cowl area) of cowl porosity at three contraction ratios of air intake have been studied. The pattern of the cowl porosity (Square shape) is chosen symmetrically along the span in the longitudinal direction from the cowl tip. Commercially available software Ansys is used in the computational studies to solve the RANS equations with the k- $\omega$  STD turbulence model. Various performance parameters of supersonic air intake are obtained and discussed. Excess amount of flow spillage appears near the cowl tip, which is responsible for the standing strong bow shock wave just before the throat for the uncontrolled case (Clean Model). The minimum energy losses and starting behavior of supersonic air intake are captured at 7.2 % cowl porosity for the contraction ratio of 1.25, which reveals the overall improvement in the flow physics and performance parameters. An increase of 32.73 % in the total pressure recovery is observed for 7.2 % cowl porosity at design contraction ratio of 1.25. All the simulations are performed at three contraction ratios of 1.22, 1.25 & 1.31.

**Keywords:** SWBLI control; Intake performance parameters; Starting behavior of intake.

### NOMENCLATURE

avg	average	P <sub>oe</sub>	total pressure at the exit of intake
FD	Flow Distortion	P <sub>o<inf></inf></sub>	free stream total pressure
H	height of the air intake	PR	pressure recovery
inf	infinite	R <sub>c</sub>	contraction ratio
L	length of air intake	w	width of the intake
M	Mach number	X	axial location in the longitudinal direction
P	local static pressure	Y	axial location in the vertical direction
P <sub>inf</sub>	free stream static pressure	Z	axial location along the span of intake

### 1. INTRODUCTION

The primary function of air intake is feeding the air to air breathing propulsion system over wide range of operation conditions, so that the engine can generate the thrust and the conditioning system can be operated. Air intake compresses the atmospheric air for high speed flights. The air, which enters the supersonic air intake is having a very high Mach number and low pressure, so it needs to be converted into low Mach number and high pressure by utilizing the air intake before feeding it to the

engine (Das and Prasad, 2010). To maximize the thrust of air breathing engine, the air intake needs to fulfill its requirements for each flight configuration and it can be achieved by maintaining low flow distortion (good homogeneity) minimum drag and shock on lip condition along with high pressure recovery (Sepahi-younsi and Feshalami, 2019). One of the simplest forms of staged compression intake is the oblique shock intake which involves oblique shocks produced by the ramp body to reduce the Mach number from the free stream value followed by a weak terminal normal shock at or near throat of intake through which flow becomes subsonic

(Neale and Lamb, 1962). Shock on lip situation is essential for most favorable intake performance, which is achieved by using the fore-body compression focused on cowl lip (Das and Prasad, 2009; Vivek and Mittal, 2009; Trapier et al. 2006). In general, the following parameters influence the air intake performance: boundary layer development, boundary layer growth due to viscous effect, shock interaction and distortion of velocity profile, movement in the normal shock position due to the mode of operation (subcritical, critical and supercritical) of the air intake is the reason behind this (Liu et al. 2017). So an air intake has to minimize shock wave and viscous losses, compress the flow proficiently and ensure the self-starting capability of intake (Soltani et al. 2015), ample angle of attack performance and nominal involvement of intake to vehicle drag (Askari et al. 2019; Reinartz et al. 2003; Fodeibou et al. 2008). So the intake aerodynamics plays a vital role and aerodynamics can be improved by making the changes in design of air intake. A detailed study on conceptual design of inverted dorsal air intake for military aircraft has been conducted by Bravo-Mosquera et al. (2019). Their aim was to study the different design configuration and find out the optimum performance by changing the shape of the diffuser from rectangular to circular end. A conceptual re-design of the air intake by using the variable ramp for B-1B bomber aircraft has been investigated by Berra et al. (2015) at a Mach number of 2.0. The Matlab, Supin and Wind-us codes were generated and validated with CFD results to develop a design process for improve the performance of the mixed compression air intake. Although the variable ramp air intake can operate for the wide range of operations but it produces an excess amount of drag and additional weight on the aircraft, which affects the overall performance of the aircraft. There are several other methods, which can be adopted to improve the overall performance and flow physics inside the supersonic air intake. Different methods have been adopted by various researchers, namely passive (Raghunathan, 1988) and active methods (Syberg and Koncsek, 1973). Bleed, Bleed with Plasma actuators (Ferrero, 2020) and boundary layer suction are some of the active methods, which are being used extensively. However, the passive methods, such as cowl deflection, (Das and Prasad, 2009), vortex generator (Lee et al. 2011), cavity (Zhuang et al. 2006), cavity with porosity (Humrutha et al. 2017), natural ventilation (Suryanarayana and Dubey, 2017), bump (Kim, et al. 2007, 2008), and air-jet (Souverein and Debièvre, 2010) are some of the techniques, which have proven themselves to overcome shock wave boundary layer interaction. A large number of studies have been reported in the literature over several years. Extensive studies on cowl lip alteration at Mach 3 to improve mass capture and combustion stability have been carried out by John and Senthilkumar (2018). Starting behavior (Tahir, 2008) of air intake with cowl deflection (zero to four degree) and boundary layer bleed is reported by Das and Prasad (2008) at designed Mach number. Effect of cavity with

porous surface on shock on cowl lip condition to minimize the SWBLI effect at three different contraction ratio for Mach 2.2 is reported by Humrutha et al. (2017). Results show a reduction in interaction losses. Effect of porous surfaces on surface pressure fluctuations, noise generation and on the boundary layer development is reported by Carlos and Silva (2017) in his comprehensive study. This study shows drop in surface pressure amplitude of 6 dB over the range of high-frequency. To assess the capability of porous medium to manage the normal-shock-wave/boundary-layer interaction (NSWBLI) for transonic speeds for aircraft wings, a computational study has been done by Roy et al. (2017). To weaken the shock structure and to reduce the wave drag, a re-circulation zone is created inside the porous medium by using passive control technique. The porous medium was created beneath the region of interaction of normal-shock-wave/boundary-layer over the flat plate and study was carried out at Mach 1.3. Some thoughts on passive control of shock boundary layer interaction by porosity have been reported by McCormick (1993) and Cerminara et al. (2018). Significant reduction in total pressure loss through the system of shock was found by the induction of isentropic compression by implementing the passive cavity with porosity. Three-dimensional flow field study of Single Expansion Ramp Nozzle (SERN) with a passive cavity has been studied by Zhou and Wang (2019). The variations in porosity percentage was a crucial factor to affect the SERN performance by adjusting separation zone size and its separation starting position, and the improvement effectiveness of the axial thrust coefficient drops with the decrease of percent of porosity. Based on the above discussion, it can be infer that by using the porosity; the impact of Shock wave boundary layer interaction can be reduced without losing the mass flow rate, without adding an additional weight and drag on the aircraft engine.

This clearly indicates the possibility of using natural ventilation as one of the passive techniques to control boundary layer separation inside air-intakes. Hardly any researcher has tried to apply the natural ventilation model in the supersonic air intake. The present study deals with an attempt to use natural ventilation on the cowl surface for possible improvement of flow field inside a mixed compression rectangular air-intake. Four different cases (percentage of porosity has been varied with respect to the total cowl area) of cowl porosity in a region of large pressure gradient especially around the throat location and just above the shock wave boundary layer interaction region have been studied. An additional objective of the present research is to identify the optimum percentage of cowl porosity. Porosity has been chosen of square shape, because of the simplicity.

## 2. GEOMETRICAL DETAILS OF MODEL

Investigations have been carried out on an air-intake designed for a contraction ratio of 1.25. The intake

has two external compression ramps, a cowl and side plates extending from the first ramp leading edge to the cowl lip. A mixed compression air intake model of designed contraction ratio of 1.25 was chosen for the present study due to the availability of computational and experimental data to validate the adopted computational approach. This model was initially proposed by [Neale and Lamb \(1962\)](#). The aim of the study was to design a mixed compression air intake for a required Mach number of 2.2 at 4 degree cowl deflection. Two different set of shock angles ( $7^\circ$ ,  $7^\circ$ ,  $10^\circ$  &  $9^\circ$ ,  $5^\circ$ ,  $10^\circ$ ) of the air intake was tested to achieve the shock on lip operation and to keep boundary layer growth minimum. These set of oblique shock were selected based on the oblique shock theory and idea was to kept the supersonic Mach no as low as possible just before the normal shock wave to achieve the high pressure recovery. In both the cases, the terminal supersonic Mach no of 1.38 was achieved, but the higher pressure recovery was achieved for the former case. Few modifications (such as the truncation in the length of the air intake) have been made by [Das and Prasad \(2010\)](#) as per their wind tunnel facility specifications in the geometry proposed by [Neale and Lamb \(1962\)](#). The angle of cowl was varied from zero to four degree in this study to capture the flow behavior of the mixed compression air intake and it was found that the intake shows the unstart behavior at zero degree cowl deflection at the design Contraction of 1.25. As the cowl deflection has been increased from 1-4 degree, the intake start showing starting behavior. So the idea of the present investigation was to achieve the starting behavior at off design condition of the supersonic air intake. Therefore, the intake cowl deflection angle was chosen to be zero degree for the present investigation. Intake geometry dimensions are shown in Fig. 1. The first ramp has a length of 9.37 mm and an angle of 7-degree with respect to the free stream direction. Second ramp has a length of 19.75 mm and an angle of 14-degree whereas after second ramp the surface has an arc of radius 16.84 mm and length 4.09 mm with respect to the free stream direction. An isolator section of 4.15 mm is at the downstream of the arc, and has two diffusers one of 26.32 mm length, at 2.31-degree angle and 31.44 mm length with a 6-degree angle. It is followed by another isolator with 35.46 mm length which continues till the exit. The sidewall of the intake starts at the first ramp and is swept at 14-degree until it meets the cowl and becomes horizontal till the exit. The cowl length starts from 22.98 mm from the first ramp and it is at a height of 14.94 mm with an external angle of 7-degree from the isolator base. The distance between the side plates is 15 mm. The sidewalls and cowl are 3 mm and 4.54 mm thick respectively. The coordinate system followed in the present study has the origin at the centre of the leading edge of the ramp bottom surface. The X-axis is taken along the length of the model, Y-axis along the height with Z-axis along the span of the intake. The dimension of each porosity block is chosen to be  $3\text{ mm} \times 3\text{ mm}$ , shown in Fig. 2. The idea behind to chose the dimension of porosity block is to make the

symmetrical pattern along the x axis. The square section has been chosen due to simplicity in meshing. Since most of the affected region by the shock wave boundary layer interaction is the throat region at the off design condition (because normal shock appear at  $X/L=0.175$ ), so the idea was to make ventilation section in the most affected region i.e. from the beginning of the cowl up-to the throat of air intake ( $X/L=0.175$  to 0.29).

The contraction ratio ( $R_c$ ) of the air intake is defined as the ratio of captured area ( $A_c$ ) to the throat area ( $A_t$ ). Contraction ratio is also the function of free stream Mach number ( $M$ ) as given by Eq. (1), which is cited by [Humrutha et al. \(2017\)](#). Contraction ratio for present study has been calculated by the following equation.

$$R_c = \frac{A_c}{A_t} = \left[ \frac{\gamma-1}{\gamma+1} + \frac{2}{(\gamma+1)M^2} \right]^{\frac{1}{2}} \left[ \frac{2\gamma}{\gamma+1} - \frac{\gamma-1}{(\gamma+1)M^2} \right]^{\frac{1}{\gamma-1}} \quad (1)$$

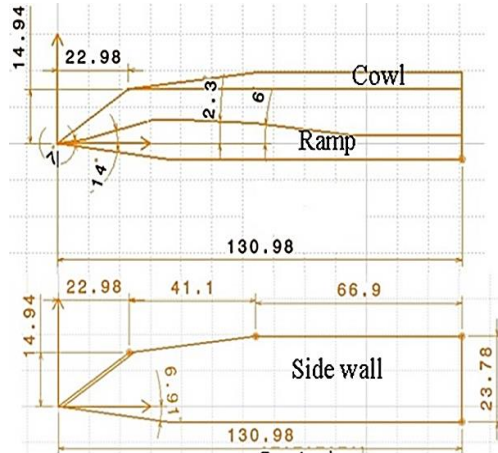


**Fig. 1. Dimension of air intake model (All the dimensions are in mm and angles are in degree).**

### 3. COMPUTATIONAL SETUP

To investigate the flow field within the intake, numerical studies were conducted using the commercially available CFD software ANSYS. All the computations were done at the central computer facility available at National Institute of Technology, Kurukshetra, Haryana. In the following sections the solution methodology, problem setup and boundary conditions are discussed in detail.

#### 3.1. Solution Methodology

Numerical simulations were performed to study the effect of cowl ventilation on the flow physics of a supersonic air intake. Finite volume technique was used to solve the Reynolds Averaged Navier Stokes equation by performing the computations. An upwind discretisation scheme with an explicit coupled solver for the convective terms and second order central differencing scheme for the diffusion terms in the flow and transport equation was

adopted. ‘ $k-\omega$  STD’ turbulence model was selected for the present investigation, which is recommended by Coratekin *et al.* (1999) for the computation of complex wall bounded high speed flow to capture the flow separation. A detailed comparison of ramp pressure distribution on symmetry plane among the turbulence model with the experimental data of Das and Prasad (2010) has been shown in Fig. 3. The variation in the position of normal shock appears for different turbulence model and high and low peak values of pressure ratio are also appeared different. Upon comparison the ramp pressure distribution for all the computed turbulence model with the experimental data of reference, a good agreement was found between the  $k-\omega$  STD model and the reference experiment. So the  $k-\omega$  STD model is chosen for the present study.

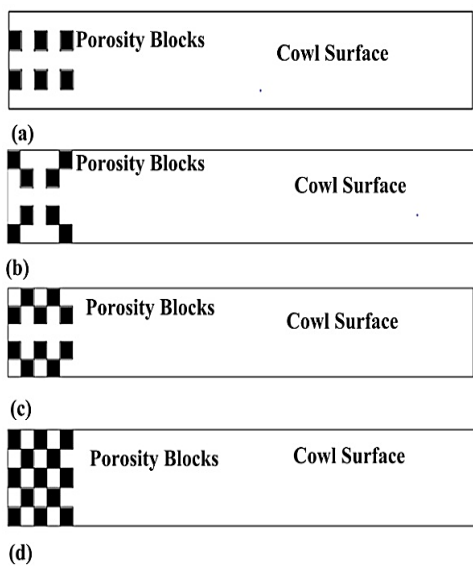


**Fig. 2. Black color shows the porosity (a) 4.4 % of total cowl area (b) 5 % of total cowl area (c) 5.5 % of total cowl area (d) 7.2 % of total cowl area. Total Cowl area is = 1620 mm<sup>2</sup>.**

Air was chosen the working fluid, which obeys the assumptions of ideal gas law. Sutherland’s law of viscosity has been used to calculate the viscosity of the fluid. Courant number of 0.8 and turbulent intensity of 5 % were selected for the fast convergence. The level of convergence was brought to  $10^{-3}$  for continuity; energy and X- velocity, while for k and omega, residual were brought to  $10^{-6}$ . Details of the number of iterations and residual values are shown in Fig. 4.

Following steps were used to setup the problem in ANSYS FLUENT: (1) defining geometry (2) meshing and checking the grid (3) selection of solver formulation and equations to be solved (laminar/turbulent/inviscid etc.) (4) Material properties (5) specification of operating and boundary conditions (6) specification of numerical properties and (7) initialization of variables.

### 3.2 Boundary Conditions

The pressure inlet boundary condition was specified to the flow facing the inlet section. To simulate the inlet Mach number of 2, 2.2 and 2.5, corresponding stagnation pressure and static pressure were provided at the inlet. Other than the inlet, all the extended domains were specified the pressure outlet boundary conditions with zero gauge pressure. No slip boundary conditions were imposed at the wall surfaces of the supersonic air intake. Pressure outlet was opted for the outflow (at the exit of the air intake) and for the porosity blocks. Gauge pressure value was given to be zero for the porosity blocks and intake exit for free flow computations. Type of boundary conditions opted for the present study are shown in Fig. 5.

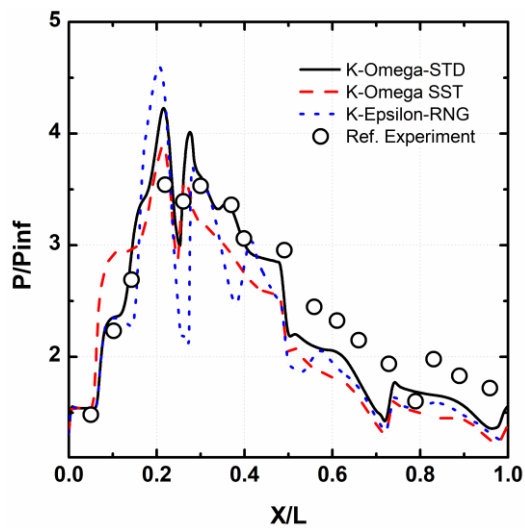


**Fig. 3. Ramp surface pressure distribution on symmetry plane for clean model.**

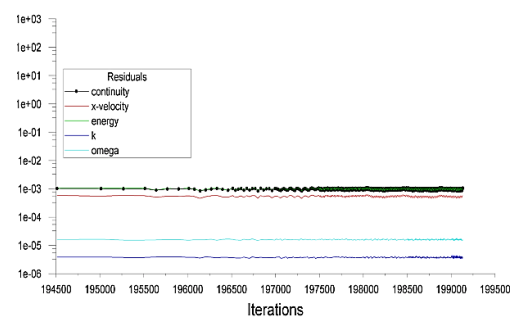


**Fig. 4. Convergence history.**

## 4. VALIDATION TEST

A confirmation test has been completed to validate the opted numerical framework for the computational simulation. Additionally, to make sure the nonexistence of grid-based inaccuracy in the numerical solution a grid independence study has to be performed. So the structured mesh was generated for all the cases and minimum spacing near the wall in y direction was chosen to be 0.001

mm. A grid containing 600000 cells was finally chosen for all the simulations based on the results obtained from grid independency test. The test was conducted for 500000 (Grid 1), 600000 (Grid 2) and 700000 (Grid 3) no of cells. Figure 6 shows the meshing details and grid independency results.

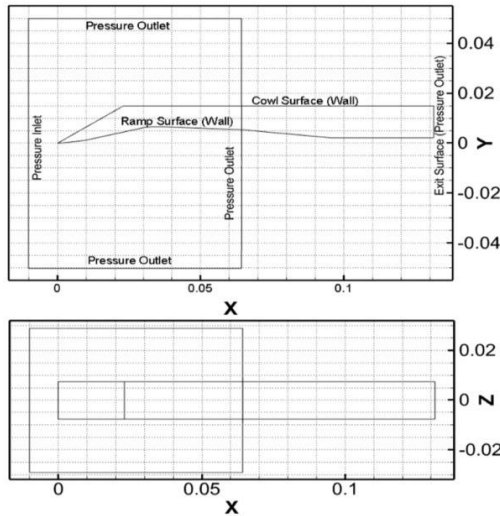


**Fig. 5. Showing details of boundary conditions along with extended domain (Dimensions are in meters).**

Static pressure distribution over the ramp and cowl surface of air intake clean (without porosity) model at zero degree cowl deflection has been computed and validated with the data obtained from Das and Prasad (2010) in Fig. 7. A good agreement of results for the cowl and ramp surface is observed, however for ramp surface, a small variation in pressure is observed from  $X/L = 0.2$  to  $0.3$ , the reason behind this is the computation in the reference paper is two-dimensional but for present computation, it is three-dimensional. Mach contours on the center plane of intake are compared with the experimental and numerical Schlieren images in Fig. 8. Oblique shock originated from the first and second ramp is not following the shock on lip condition, resulting in bow shock formation near the cowl tip and flow spillage along with the separation of flow is also observed in Mach contours and Schlieren image.

## 5. RESULTS AND DISCUSSION

The present study investigates the efficacy of cowl porosity on performance of air intake, particularly on SWBLI inside the air intake at design Mach no 2.2 and additionally at two other Mach numbers of 2 and 2.5. Four cases of cowl porosity have been investigated for three contraction ratios ( $R_c$ ) of 1.22, 1.25 and 1.3. Static pressure distribution on ramp and cowl surface and distribution of total pressure at the intake exit on symmetry plane have been drawn against the longitudinal and vertical axis respectively. The calculated pressure ( $P$ ) is made non-dimensional with free stream pressure

( $P_{inf}$ ) and axial distance ( $X$ ) is made non-dimensional with length ( $L$ ) of the intake. Similarly, the vertical distance ( $Y$ ) is made non-dimensional with height ( $H$ ) of the intake and total exit pressure ( $P_{oe}$ ) with free stream total pressure ( $P_{0inf}$ ). Mach contours are also investigated to study the flow pattern inside the air intake. All the simulations are carried out at supersonic exit Mach number. Detailed discussion on the obtained results is presented in the next section.

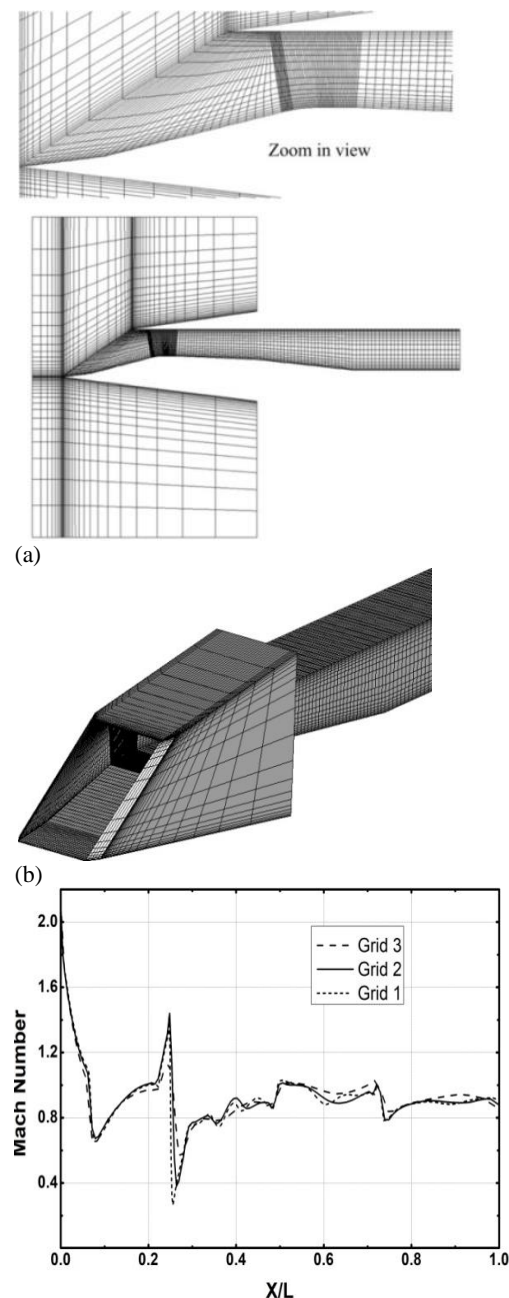


**Fig. 6. Showing sample mesh for air intake model & grid independency test (a) Centre plane view (b) Surface grid (c) Mach number distribution on-ramp surface.**

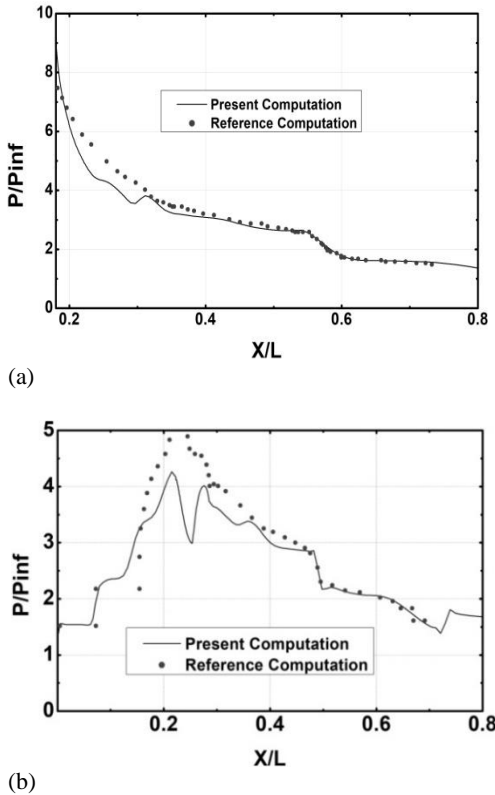


**Fig. 7. Pressure distribution along the length of intake for clean model (a) Cowl surface (b) Ramp surface.**

An assessment of distribution of static pressure on the cowl surface is shown in Fig. 9 for  $R_c$  equal to 1.22, 1.25 and 1.31. The pressure distribution pattern for the uncontrolled (clean model) cases are similar, however, the pressure is higher at the cowl tip for  $R_c$  equal to 1.22 and it must be because of the appearance of the strong bow shock around the cowl lip and larger amount of flow spillage. The maximum value of cowl pressure is obtained at  $X/L = 0.2$  and it shows that the intake is in unstart condition for all the uncontrolled cases. Huge fluctuation in pressure can be seen from  $X/L = 0.18$  to 0.30 for all the controlled cases and this is because of the suction effect of porosity. From  $X/L = 0.3$  onwards, as the porosity increases, the pressure along the cowl surfaces for the entire remaining length decreases in the order of increasing in porosity for all the three cases of contraction ratio.

Observations of pressure distribution on-ramp surface at symmetry plane are plotted in Fig. 10 for all contraction ratios. The pattern of pressure distribution for the uncontrolled cases are exactly same for  $R_c = 1.22$  and 1.25, except for  $R_c = 1.31$ . Pressure remains constant for the first ramp and then a jump in the pressure is observed owing to the generation of oblique shock from the second ramp. Thereafter pressure rises due to the strong bow shock and flow spillages for  $R_c = 1.22$  & 1.25. However, for  $R_c = 1.31$ , the pressure remains constant for the second ramp as well and then decreases because of the weak oblique shock appearance in the throat of air intake. This unstart

behavior of air intake is witnessed for all the uncontrolled cases. Pressure pattern is observed as expected for the first and second ramp due to oblique shock formation from the first and second ramp. Thereafter significant difference in flow characteristics can be noticed for all the controlled cases. From  $X/L = 0.2$  onwards, there is a drop and rise in the pressure amplitude, which indicates the conversion of strong bow shock into the oblique shock around the cowl lip and throat of the air intake. Upon proceeding further towards the end of air intake, proper diffusion of the flow inside the duct can be noticed for all the controlled cases as compared with the uncontrolled case. The exit value of pressure ratio is equal to one for all three cowl porosity models except cowl porosity of 7.2 % at contraction ratio of 1.22. But in case of contraction ratio of 1.25 and 1.31, all the exit values of pressure ratio are greater than one except 7.2 % cowl porosity at 1.25 contraction ratio. This is the designed contraction ratio of air intake. Although all the controlled cases show starting behavior for contraction ratio of 1.31 but among all the simulated cases, superior performance is achieved at 7.2 % cowl porosity for contraction ratio of 1.25 and intake shows the starting characteristic.

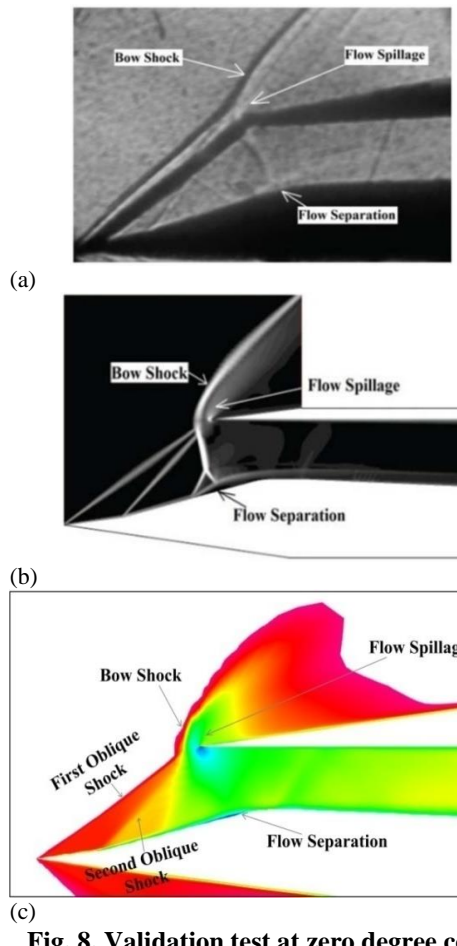


**Fig. 8. Validation test at zero degree cowl deflection (a) Schlieren image -Das and Prasad (2010) (b) Numerical Schileren-Das and Prasad (2010) (c) Mach contour-Present computation.**

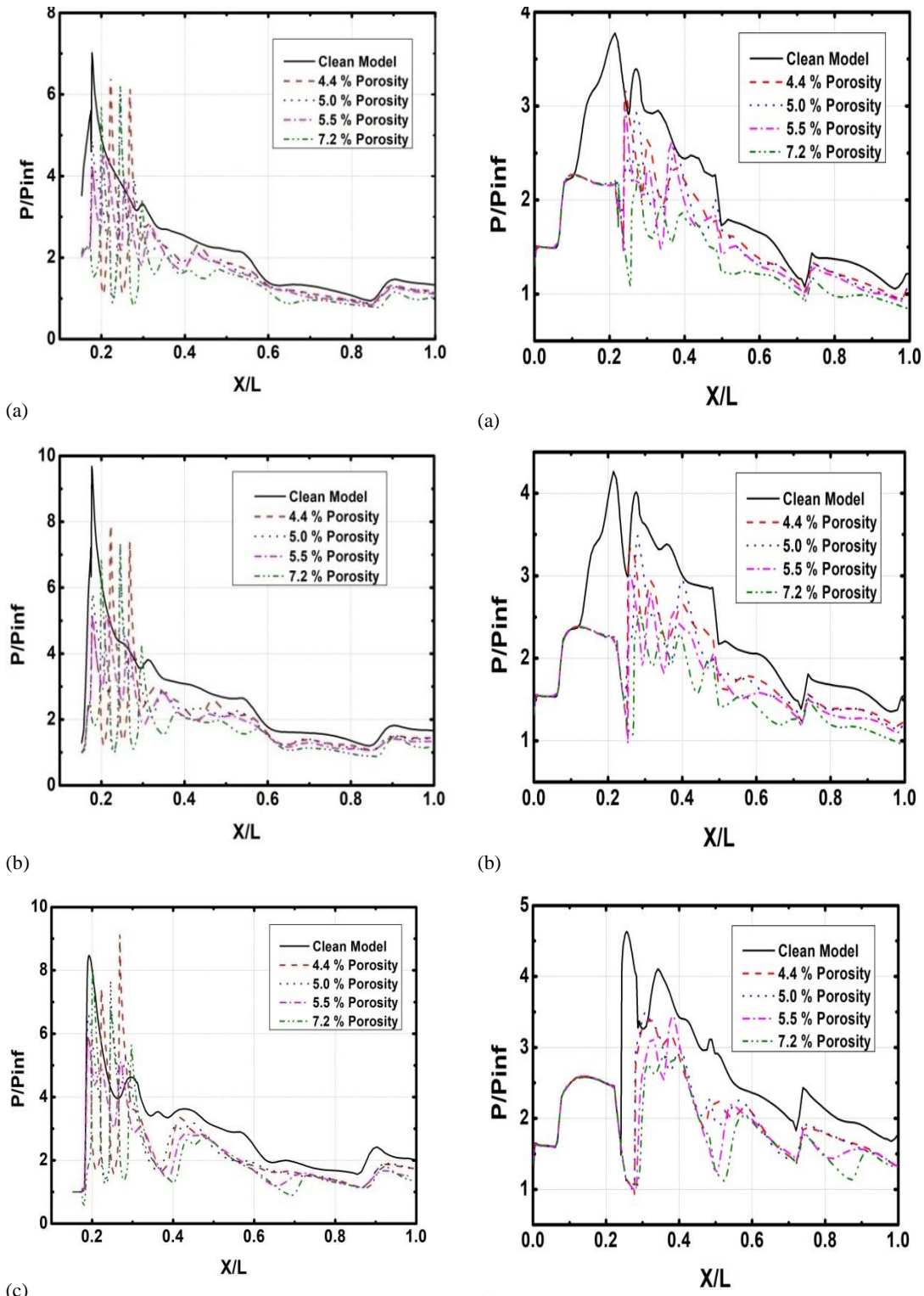


**Fig. 9. Static pressure comparison on cowl surface at symmetry plane (a)  $R_c = 1.22$  (b)  $R_c = 1.25$  (c)  $R_c = 1.31$ .**

plotted against  $Y/H$  in Fig. 11. Significant improvements in total pressure ratio can be noted for all controlled cases at all contraction ratio. The maximum value of total pressure is obtained for 7.2 % cowl porosity and minimum value is reported for

To assess the performance of air intake, one should always calculate the total pressure ratio at the intake exit. Total pressure ratio on symmetry plane ( $Z/W=0$ ) at the exit ( $X/L=1$ ) of the air intake is

**Fig. 10. Static pressure comparison on-ramp surface at symmetry plane (a)  $R_c = 1.22$  (b)  $R_c = 1.25$  (c)  $R_c = 1.31$ .**

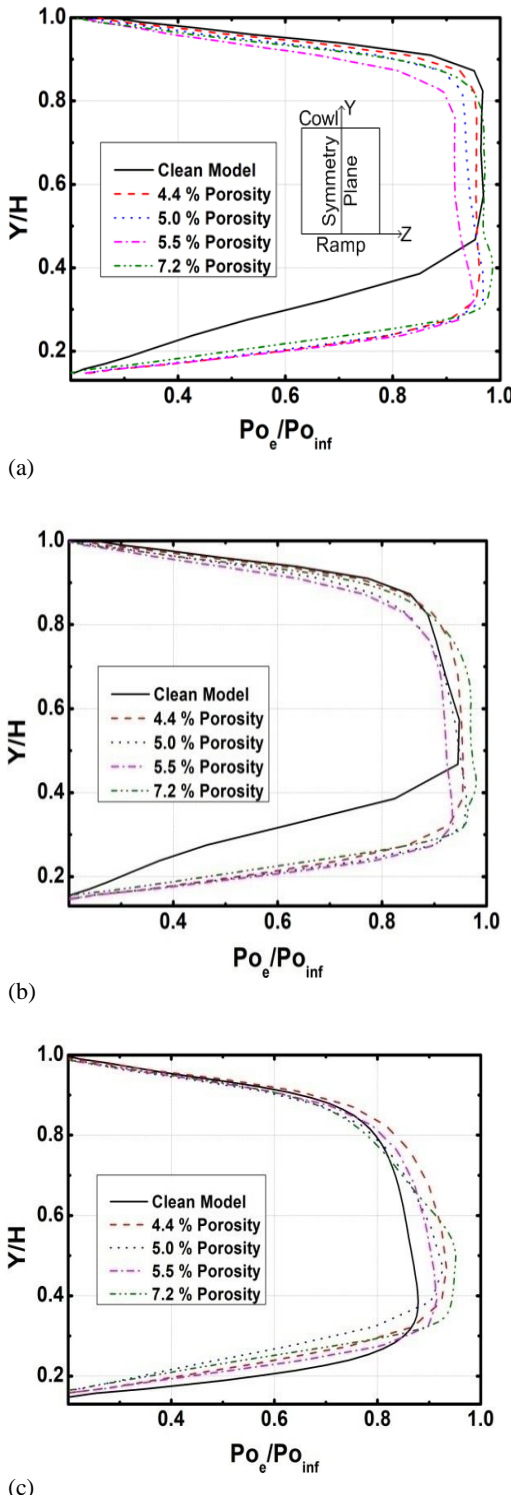


**Fig. 11. Total pressure comparison at symmetry plane on intake exit ( $X/L=1$ ) (a)  $Rc = 1.22$  (b)  $Rc = 1.25$  (c)  $Rc = 1.31$ .**

5.5 % cowl porosity, however, the remaining two cases show the average rise. Improvements in flow with cowl porosity are noted towards the ramp side only for contraction ratio of 1.22 and 1.25. But optimum performance comes with cowl porosity of 7.2 % at designed contraction ratio.

To validate the above statements regarding the superior performance of supersonic air intake, comparison of Mach contours for all the cases of cowl porosity has been shown in Fig. 12 for Mach 2, 2.2 and 2.5. All the Mach contours images are truncated at  $X/L = 0.5$ . To achieve the starting characteristic of a supersonic air intake, following criteria need to be satisfied. Oblique shocks originated from the first and second ramp should hit the cowl lip to achieve the cowl on lip condition and then the reflections of those oblique shocks should appear inside the duct for internal compression of the flow. Such conditions did not observe for uncontrolled cases (at Mach 2 & 2.2) and flow spillage near the cowl lip with a standing bow shock is clearly seen. This leads to the flow separation at the throat. While oblique shock appeared at the throat but further reflection inside the duct is missing for Mach 2.5.

The effect of cowl porosity on internal flow physics of supersonic air intake along with weak shock appearance due to suction effect of porosity is observed in all the controlled cases. Shock on lip condition and then shock reflection inside the duct at 7.2 % cowl porosity is seen for Mach 2.2. While for Mach 2.5, starting behavior of air intake on all the controlled cases is found.

Pressure recovery (PR) and flow distortion (FD) are two important performance parameters of supersonic air intake. Larger should be the value of pressure recovery and lesser should be the flow distortion. Values of these performance parameters have been calculated by using the Eqs. (2) & (3) and are shown in table 1 & 2 respectively.

$$PR = \frac{P_{oe\text{avg}}}{P_{o\text{inf}}} \quad (2)$$

$$FD = \frac{P_{oe\text{max}} - P_{oe\text{min}}}{P_{oe\text{avg}}} \quad (3)$$

PR and FD calculations reveal that the flow inside the duct for controlled cases is improved significantly for contraction ratio of 1.22 and 1.25. For 1.31 contraction ratios, the FD increases for all the controlled cases, while PR decreases for the first three controlled cases (4.4 %, 5 % & 5.5 % porosity) and 11.86 % increment is calculated for 7.2 % cowl porosity.

**Table 1 Summary of Pressure Recovery**

Cases	PR		
	$Rc = 1.22$	$Rc = 1.25$	$Rc = 1.31$
Without Porosity	0.6075	0.5621	0.6647
4.4 % Cowl Porosity	0.6809	0.6429	0.5682
4.8 % Cowl Porosity	0.6634	0.6289	0.5200
5.5 % Cowl Porosity	0.6393	0.6161	0.5578
7.2 % Cowl Porosity	0.8551	0.8356	0.7542

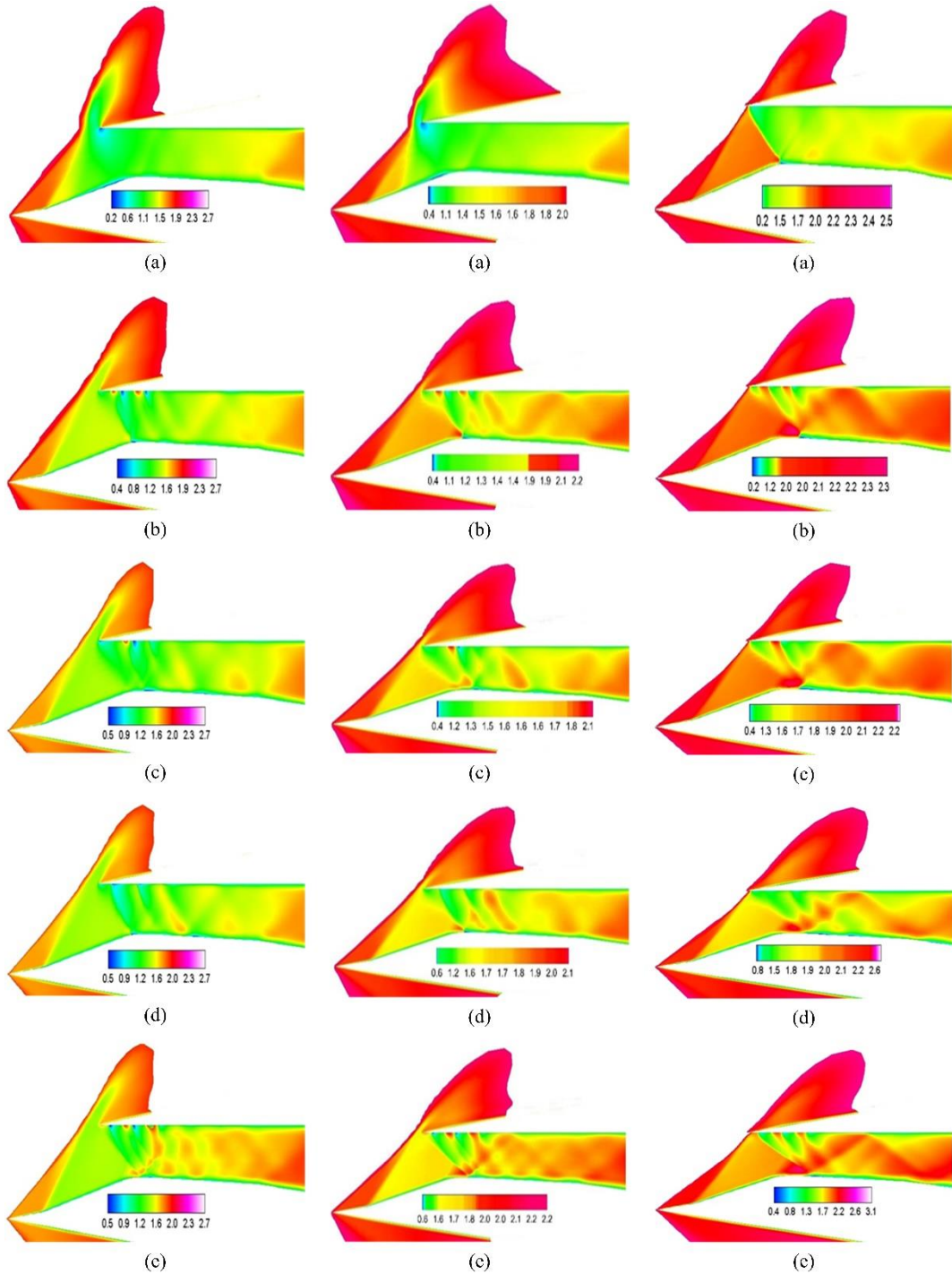


**Fig. 12. Mach Number contours at Mach 2, 2.2 & 2.5 respectively (starting from the left) (a) CleanModel- uncontrolled case (b) 4.4 % Cowl porosity (c) 5 % Cowl porosity (d) 5.5 % Cowl porosity (e) 7.2 % Cowl porosity.**

## 1. CONCLUSION

Hence the optimum condition is achieved at the design contraction ratio of 1.25 with cowl porosity of 7.2 %, because the PR is increased by 32.73 % and FD is decreased by 39 %. Table 3 and 4 shows the % difference in the PR & FD for all the controlled cases with reference to the clean model respectively. Negative sign indicates the reduction in parameter while the positive sign indicates the increment in performance parameter.

Three-dimensional qualitative and quantitative simulations have been executed to study flow physics within the supersonic air intake at various contraction ratio with and without cowl ventilation. The main objective of this study was to make the intake start at off design condition and it has been achieved for all the controlled cases of  $R_c = 1.31$  and 7.2 % cowl porosity case at  $R_c = 1.25$ , however

at  $R_c = 1.22$  for all the controlled cases; intake shows the unstart phenomena. Significant increment in the performance parameters has been observed at  $R_c=1.22$ , while reduction has been calculated for first three cases at  $R_c=1.31$  and a little increment is observed for 7.2 % cowl porosity case. A superior performance has been reported for 7.2 % cowl porosity at  $R_c = 1.25$ . Hence by controlling the percentage of porosity the flow filed inside the duct can be controlled. The results from the present study indicate that the cowl porosity method could be utilized to address the starting problem of the air intake and the performance of the mixed compression air intake can also be improved. In future studies the effect of back pressure can be investigated on the presented configurations.

**Table 2 Summary of Flow Distortion**

Cases	FD		
	$R_c = 1.22$	$R_c = 1.25$	$R_c = 1.31$
Without Porosity	1.255	1.347	1.036
4.4 % Cowl Porosity	1.068	1.166	1.376
4.8 % Cowl Porosity	1.115	1.207	1.520
5.5 % Cowl Porosity	1.149	1.206	1.376
7.2 % Cowl Porosity	0.9215	0.969	1.085

**Table 3 Comparison of % difference of pressure recovery (PR) with reference to the clean model**

Cases	% difference in PR		
	$R_c = 1.22$	$R_c = 1.25$	$R_c = 1.31$
4.4 % Cowl Porosity	+10.77	+12.56	-16.98
4.8 % Cowl Porosity	+8.42	+10.62	-27.82
5.5 % Cowl Porosity	+4.97	+8.76	-19.16
7.2 % Cowl Porosity	+28.95	+32.73	+11.86

**Table 4 Comparison of % difference of flow distortion (FD) with reference to the clean model**

Cases	% difference in FD		
	$R_c = 1.22$	$R_c = 1.25$	$R_c = 1.31$
4.4 % Cowl Porosity	-17.50	-15.52	+24.7
4.8 % Cowl Porosity	-12.55	-11.59	+31.84
5.5 % Cowl Porosity	-9.22	-11.69	+24.7
7.2 % Cowl Porosity	-32.39	-39	+4.51

#### ACKNOWLEDGMENTS

Authors acknowledge support of department of mechanical engineering of NIT Kurukshetra and

SRM IST for providing their kind support throughout this work.

#### REFERENCES

- Askari, R., M. R. Soltani, K. Mostoufi, A. K. Fard and M. Abedi (2019). Angle of attack investigations on the performance of a diverterless supersonic inlet. *Journal of Applied Fluid Mechanics* 12 (6), 2017–30.
- Berra, L. M., John W. Slater and Semih M. Olcmen (2015). Conceptual Redesign of the B-1B Bomber Inlets for Improved Supersonic Performance. *Aerospace Science and Technology* 45, 476–83.
- Bravo-Mosquera, P. D., A. M. Abdalla, H. D. Cerón-Muñoz and F. M. Catalano (2019). Integration Assessment of Conceptual Design and Intake Aerodynamics of a Non-Conventional Air-to-Ground Fighter Aircraft. *Aerospace Science and Technology* 86, 497–519.
- Cerminara, A., R. Deiterding and N. Sandham (2018). DNS of hypersonic flow over porous surfaces with a hybrid method. *2018 AIAA Aerospace Sciences Meeting*, no. January: 1–24.
- Coratekin, T., J. V. Keuk, and J. Ballmann (1999). Preliminary investigations in 2d and 3d ramjet inlet design. *AIAA Journal* 99 (2667), 1–11.
- Das, S. and J. K. Prasad (2008). Characteristics of a supersonic air-intake with bleed. In *Proceedings of the International Conference on Aerospace Science and Technology*, 26–28 June 2008, Bangalore, India, 2–5.
- Das, S. and J. K. Prasad (2009). Cowl deflection angle in a supersonic air intake. *Defence Science Journal* 59 (2), 99–105.
- Das, S. and J. K. Prasad (2010). Starting characteristics of a rectangular supersonic air-intake with cowl deflection. *The Aeronautical Journal* 114 (February), 177–89.
- Ferrero, A. (2020). Control of a Supersonic Inlet in Off-Design Conditions with Plasma Actuators and Bleed. *MDPI* 7 (32), 1–26.
- Fodeibou, T., Z. Huque and J. Galvis (2008). Effects of mach number and angle of attack on mass flow rates and entropy gain in a supersonic inlet. *World Academy of Science, Engineering and Technology* 46, 541–44.
- Humrutha, G., M. Kaushik and K. P. Sinhamahapatra (2017). Shock boundary layer interaction control in supersonic intake using cavity with porous surface. *35th AIAA Applied Aerodynamics Conference*, no. June: 1–8.
- Carlos, R. and I. D. Silva (2017). Boundary layer flow interaction with porous surfaces. *24th International Congress on Sound and*

- Vibration, ICSV 2017, 1–8.
- John, B. and P. Senthilkumar (2018). Alterations of cowl lip for the improvement of supersonic-intake performance. *Journal of Applied Fluid Mechanics* 11 (1), 31–41.
- Kim, S. D. and D. J. Song (2008). Numerical study on performance of supersonic inlets with various three-dimensional bumps. *Journal of Mechanical Science and Technology* 22 (8), 1640–47.
- Kim, S. D., D. J. Song and S. Lim (2007). A numerical analysis on three-dimensional flow field in a supersonic bump inlet. In *Collection of Technical Papers - 45th AIAA Aerospace Sciences Meeting*, 12:8534–41.
- Lee, S., E. Loth and H. Babinsky (2011). Normal shock boundary layer control with various vortex generator geometries. *Computers and Fluids* 49 (1), 233–46.
- Liu, J., H. Yuan, and N. Ge (2017). The Flowfield and Performance Analyses of Turbine-Based Combined Cycle Inlet Mode Transition at Critical/Subcritical Conditions. *Aerospace Science and Technology* 69, 485–94.
- Mccormick, D. C. (1993). Shock/boundary-layer interaction control with vortex generators and passive cavity. *AIAA Journal* 31 (1), 91–96.
- Neale, M. C. and P. S. Lamb (1962). Tests with a variable ramp intake having combined external/internal compression, and a design mach number of 2.2. *Aeronautical Research Council, CP-805* 1–35.
- Raghunathan, S. (1988). Passive control of shock-boundary interaction. *Progress in Aerospace Sciences* 25, 271–96.
- Reinartz, B. U., D. Carsten, Herrmann, J. Ballmann and W. W. Koschel (2003). Aerodynamic performance analysis of a hypersonic inlet isolator using computation and experiment. *Journal of Propulsion and Power* 19 (5), 868–75.
- Roy, S., K. Subramaniam and S. Ghosh. (2017). Passive control of normal-shock-wave/boundary-layer interaction using porous medium: computational study. *35th AIAA Applied Aerodynamics Conference*, no. June.
- Sepahi-younsi, J. and B. F. Feshalami (2019). Performance evaluation of external and mixed compression supersonic air intakes: parametric study. *Journal of Aerospace Engineering* 32 (5), 1–14.
- Soltani, M. R., J. S. Younsi and V. F. Khanapostani (2015). Numerical investigation of the unstart suppression in a supersonic air intake. *Iranian Journal of Science and Technology - Transactions of Mechanical Engineering* 39 (M2), 413–26.
- Souverein, L. J. and J. F. Debièvre (2010). Effect of air jet vortex generators on a shock wave boundary layer interaction. *Experiments in Fluids* 49 (5), 1053–64.
- Suryanarayana, G. K. and R. Dubey. (2017) Image analyses of supersonic air-intake buzz and control by natural ventilation. *Journal of Visualization* 20 (4), 711–27.
- Syberg, J. and J. L. Koncsek (1973). Bleed system design technology for supersonic intakes. *Journal of Aircraft* 10 (7), 407–13.
- Tahir, R. (2008). *Analysis of shock dynamics in supersonic intakes*. Ph. D. thesis, McGill University, Montreal, Quebec, Canada.
- Trapier, S., P. Duveau and S. Deck (2006). Experimental study of supersonic inlet buzz. *AIAA Journal* 44 (10), 2354–65.
- Vivek, P. and S. Mittal (2009). Buzz instability in a mixed-compression air intake. *Journal of Propulsion and Power* 25 (3), 819–22.
- Zhou, L. and Z. Wang. (2019) Numerical investigation on the three three-dimensional flow flowfield in the single expansion ramp nozzle with passive cavity flow control. *Journal of Applied Fluid Mechanics* 12 (4), 1115–26.
- Zhuang, N., F. S. Alvi, M. B. Alkislar and C. Shih (2006). Supersonic cavity flows and their control. *AIAA Journal* 44 (9), 2118–28.